JOURNAL OF MATERIALS SCIENCE: MATERIALS IN MEDICINE 4 (1993) 292–295

A pyrolytic route for the formation of hydroxyapatite/fluoroapatite solid solutions

UWE PARTENFELDER, ANGELA ENGEL, CHRISTIAN RÜSSEL
Institut für Werkstoffwissenschaften III (Glas und Keramik), Universität Erlangen, 852 Erlangen, Martensstr. 5, Germany

Pyrolytic routes previously developed for the formation of hydroxyapatite and calciumfluoride were modified and combined for the formation of hydroxyapatite/fluoroapatite solid solutions. Hereby phenyldichlorophosphine, calcium nitrate and calcium trifluoroacetate were used as starting materials. Hydrolysis and oxidation led to a polycondensation and enabled the formation of a viscous solution which, by means of drying, could be transformed to an amorphous solid. Calcining of this solid at temperatures up to 1100 °C led to the formation of hydroxyapatite/fluoroapatite solid solutions.

1. Introduction

Calcium phosphates, because of their chemical composition, roughly equivalent to the inorganic matrix of the human bone, are most suitable for implant materials [1–3]. The inorganic matrix is based on hydroxyapatite, $Ca_{10}(PO_4)_6(OH)_2$ doped with different quantities of Na^+, K^+ and Mg^{2+} which occupy Ca^{2+} sites, and anions, such as CO_3^{2-}, SO_4^{2-} and F^-, substituting OH^--groups. These dopants, especially F^- exercise a great influence on the physical and biological properties of the material [4–6].

In contrast to metals or bio-inert ceramics where an encapsulation takes place, hydroxyapatite is not only biocompatible but also bioactive, because of its direct bonding to the bone [7–9].

Hydroxyapatite forms solid solutions with fluoroapatite [10]. Their lattice parameters are approximately the same (hydroxyapatite (ASTM card No.: 9-432): $a_0 = 0.9418$ nm, $c_0 = 0.6884$ nm; fluoroapatite (ASTM card No.: 15-876): $a_0 = 0.9364$ nm, $c_0 = 0.6884$ nm). Fluorine doped hydroxyapatite possesses a notably higher corrosion resistance especially in biological environment [11]. The crystallization of rapidly quenched calcium phosphates is promoted in the presence of fluorine. In particular, if plasma sprayed coatings are used, a higher degree of crystallization, and hence mechanical strength, is realized [12].

Stoichiometric fluoroapatite possesses a fluorine content of 3.77 wt %, the fluorine content of the human bone is around 1 wt % [12]. Implant materials should not exhibit notably higher fluorine concentrations otherwise toxic reactions cannot be avoided.

The preparation of hydroxyapatite by a polymeric route has been described [13], as has the preparation of calcium fluoride using the thermal decomposition of calcium trifluoroacetates [14]. In this study, these two routes were modified and combined, leading to a pyrolytic route enabling the preparation of hydroxyapatite/fluoroapatite solid solutions with exact stoichiometry.

2. Experimental procedure

Fig. 1 shows a flow diagram of the pyrolytic route used. Calcium trifluoroacetate was prepared by dissolving calcium carbonate with trifluoroacetic acid as previously described [14]. Water and excess acid were evaporated and after drying at 90 °C, the obtained salt, $Ca(CF_3COO)_2 \cdot xH_2O$, possessed a water content of 3.3 wt %.

Phenyldichlorophosphine, $C_6H_5PCl_2$, was mixed with acetone and carefully hydrolyzed with water [13]. A solution of an exact stoichiometric quantity of calcium nitrate, $Ca(NO_3)_2$, and calcium trifluoroacetate, $Ca(CF_3COO)_2$, in acetone was added under continuous stirring. Air was bubbled through the solution in order to oxidize the phosphorous (III) to phosphorous (V) compounds. After stirring for 1 h at 40 °C, a considerable increase in viscosity was observed. Further heating to 70 °C led to the evaporation of the solvent and, subsequently, of nitric gases. The obtained solid was dried at 110 °C and subsequently calcined in air at temperatures up to 1100 °C.

The intermediates and products obtained were characterized using X-ray diffraction (XRD) (Siemens D500), Fourier transform infrared spectroscopy (FTIR) (Mattson Polaris), thermogravimetry (TGA) (Netzsch STA 409, applied heating rate: 2 K min^{-1}) and scanning electron microscopy (SEM) (Cambridge). The fluorine content of the apatite was determined with the aid of a fluorine sensitive electrode (Ingold) after dissolution of the apatite in nitric acid using appropriate conditioners [15].

3. Results and discussion

Hydrolysis, condensation and oxidation of phenyldichlorophosphine has already been discussed [13], mainly based on the corresponding infrared spectra:

$$C_6H_5 - PCl_2 + H_2O \rightarrow C_6H_5 - P(OH)_2 + 2\,HCl \quad (1)$$

0957–4530

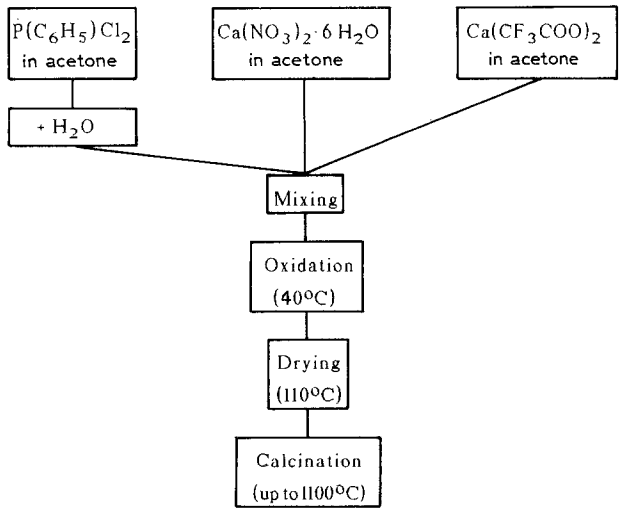

Figure 1 Flow diagram for the preparation of hydroxyapatite/fluoroapatite solid solutions.

$$C_6H_5 - P(OH)_2 \xrightarrow[-H_2O]{+O_2} 1/n \left[\begin{array}{c} C_6H_5 \\ | \\ -P-O- \\ \| \\ O \end{array} \right]_n \quad (2)$$

Fig. 2 graph (a) shows a TGA profile of the dried polymeric compound prepared with the addition of calcium nitrate (without calcium trifluoroacetate). A weight loss of about 4% was observed at a temperature of around 150 °C, and about 10% weight loss was seen at temperatures in the range 350–400 °C, further slight weight loss even at temperatures above 800 °C. The ceramic yield was 82%. Fig. 2 graph (c) shows a TGA-profile of calcium trifluoroacetate. At around 140 °C, a weight loss of 4%, due to the evaporation of water, and at about 300 °C, a steep decrease in weight was observed. The total weight loss was 77.7%. Fig. 2 graph (b) presents a TGA profile of the dried polymeric compound prepared with the addition of 23 wt % $Ca(CF_3COO)_2$. At around 150 °C, a weight loss of 4.5% was observed. Further weight loss occurred in the range of 280–300 °C. The ceramic yield in this case was 70%. This is in fairly good agreement with the weight loss of 31% calculated from Fig. 2 graph (a) and (c), and the chemical composition of the sample.

DTA profiles of the three compounds are shown in Fig. 3. The weight losses at temperatures in the range of 120–160 °C correspond to an endothermic reaction, supposedly due to the evaporation of residual water and solvent. The main weight losses at temperatures in the range of 280–400 °C correspond to highly exothermic reactions. Fig. 3 curves (a) and (c) show additional, relatively broad and exothermic peaks in the range 600–850 °C. The thermal decomposition of calcium trifluoroacetate has already been reported in [14]:

$$Ca(CF_3COO)_2 \xrightarrow{280\,^\circ C} CaF_2 + \text{volatile compounds} \quad (3)$$

The ceramic yield of 21.7% calculated from Equation

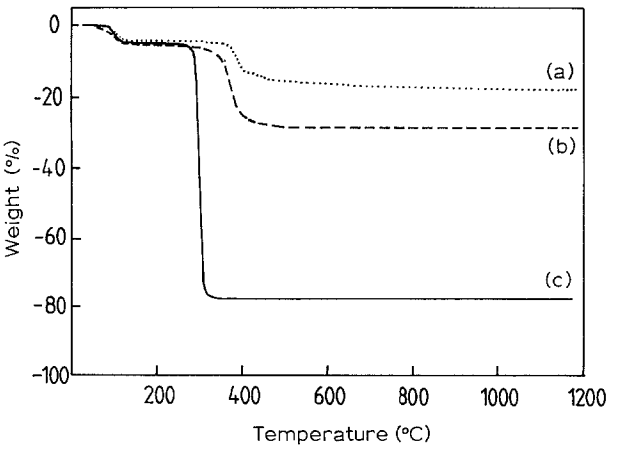

Figure 2 TGA profile of (a) dried polymer (without calcium trifluoroacetate); (b) dried polymer with the addition of calcium trifluoroacetate; (c) calcium trifluoroacetate.

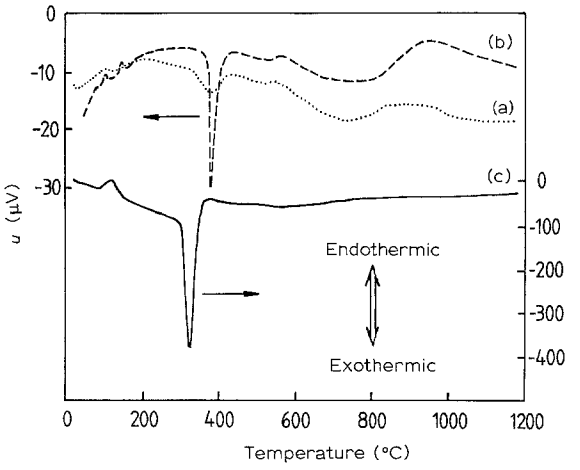

Figure 3 DTA profile of (a) dried polymer (without calcium trifluoroacetate); (b) dried polymer with the addition of calcium trifluoroacetate; (c) calcium trifluoroacetate.

3 coincide fairly well with the weight loss in the TGA profile of 77.7%. Although the thermal decomposition of pure calcium trifluoroacetate occurred at notably lower temperatures than that of the fluorine-free polymer (Figs 2 and 3, graphs (b), fluorine doped polymers (Figs. 2 and 3 graphs (c)) are not pyrolyzed in two steps. Obviously, the decomposition of trifluoroacetate is hindered in the presence of the phosphorous containing polymer.

Fig. 4, graph (a) shows an FTIR spectrum of a dried polymer. The broad absorption at 3000 to 3700 cm^{-1} is due to the ν_{O-H} vibration. Lines related to the phenyl group can be seen at 1400–1500 cm^{-1} ($\nu_{C=C}$), 690–750 cm^{-1} (δ_{C-H} (out of plane) and δ_{ring}). The broad absorption at around 500–600 cm^{-1} is due to the phosphorous–phenyl vibration. Lines related to P = O and P–O bonds are observed at 1100 and 900 cm^{-1}, respectively. The sharp line at 1384 cm^{-1} is due to the ν_{N-O} vibration and the relatively broad absorption at 1620 cm^{-1} is due to $\nu_{N=O}$ and $\nu_{C=O}$. Calcination temperatures up to 250 °C did not lead to notable changes in the FTIR spectra. At a calcination temperature of 330 °C (see graph (b)), the intensity of lines related to the phenyl group as well as that at

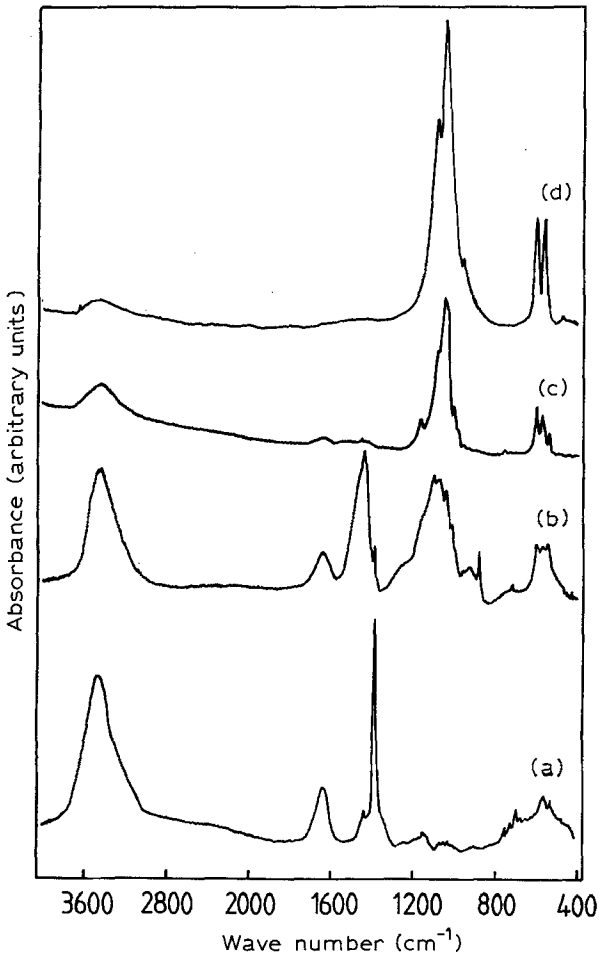

Figure 4 FTIR spectra of (a) the dried calcium trifluoroacetate containing precursor; samples calcined at (b) 330 °C; (c) 480 °C; (d) 1100 °C (fluorine content after calcination 0.16 wt %; soak 5 h).

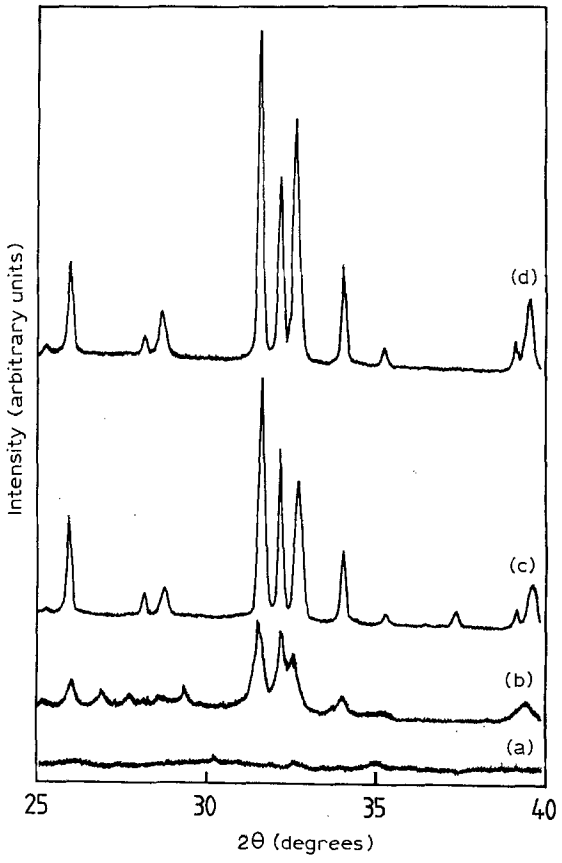

Figure 5 XRD patterns of samples calcined at different temperatures: (a) 280 °C; (b) 380 °C; (c) 780 °C; (d) 1100 °C (fluorine content after calcination 1.88 wt %; soak 5 h).

1384 cm^{-1} attributed to the N–O group decreased drastically. The lines due to the $\nu_{P=O}$ vibration (1100 cm^{-1}) and the ν_{P-O} vibration (900 cm^{-1}), however, showed notably higher intensity. Calcining at a temperature of 480 °C led to a nearly complete removal of all organic compounds, the spectra obtained are fairly similar to those obtained at higher calcination temperatures, e.g. at 1100 °C (graph (d)). The sharp line at 3500 cm^{-1} is due to non-bridging O–H.

The polymeric precursor and products calcined at temperatures up to 280 °C are amorphous (Fig. 5, graph (a)). Calcining at 380 °C led to a crystalline product; the corresponding XRD patterns show notably broadened lines, either due to small crystallites or a highly distorted lattice. Samples calcined at higher temperatures (Fig. 5 graph (c) and (d) for calcination temperatures of 780 and 1100 °C, respectively) showed XRD patterns possessing more narrow lines. The 2Θ-values of the lines in Fig. (5), graphs (b)–(d), however, are very similar and, despite slight shifts, match those of commercially available hydroxyapatite or fluoroapatite. Lines attributable to other calcium phosphates, such as tricalcium phosphate or calcium fluoride, were not observed.

According to the FTIR spectra, the phosphorous–phenyl bond is not destroyed during drying and calcining at temperatures up to 280 °C. Therefore, Equation 4 may be suggested as follows:

$$6\,PO_2C_6H_5\cdot(10-x)CaO\cdot xCa(CF_3COO)_2 \xrightarrow[-\text{ organic}]{+\,O_2} Ca_{10}(PO_4)_6(OH)_{2-2y}F_{2y} \quad (4)$$

It should be noted that the ceramic yield of 85.5% for pure hydroxyapatite ($x = 0$) calculated from Equation 4 coincides very well with the TGA weight loss of 14% experimentally observed for a polymer dried at 250 °C.

If calcium trifluoroacetate acted in the pure compound as well as in the phosphorous-containing polymer as fluorinating agent in the quantitatively same manner, Equation 4 should be written with $x = y$. Chemical analysis, however, resulted in notably lower fluorine contents in the range $y = 0.46x$ to $0.54x$: this means that the fluorine content of the apatite was around half the value predicted from Equation 3 from the concentration of trifluoroacetate added. It should be noted that the fluorine content did not depend on the soaking time or the calcination temperature.

XRD patterns and FTIR spectra of samples calcined at differnt temperatures are in agreement with the TGA and DTA profiles. The main weight loss, observed at about 400 °C is due to evaporation (and oxidation) of the major quantity of organic compounds. At higher calcination temperatures, the FTIR spectra indicate only minor quantities of organic compounds and the XRD patterns are equal to those of hydroxyapatite and fluoroapatite. The broad exothermic peak observed in the DTA profile at a temper-

ature of 700 °C corresponds to the line-narrowing in the XRD patterns and hence is attributable to the crystallization of apatite. In the fluorine-doped sample, this peak is sharper and occurs at slightly lower temperatures.

Fig. 6 shows XRD patterns of samples calcined at 1100 °C possessing different fluorine contents. By comparison with the XRD patterns of commerically available hydroxyapatite or fluoroapatite, the lines are considerably shifted. Compared with the lattice constants given in the literature, lines possessing high l-indices and low h and k indices are shifted towards lower 2 Θ values and hence the apatite lattice proved to be distorted. From the Miller (hkl) indices, the lattice constants can be calculated. With increasing calcination temperature and soaking time, the calculated lattice constants become closer and closer to those reported in the ASTM card. As shown in Fig. (6), the XRD patterns also depend on the quantity of fluorine in the lattice. Fig. 6 curve (c) (fluorine content: 0.6 wt%) shows three intensive peaks in the 2Θ range 31–33°. These peaks are attributable to the [300], [112] and [211] Miller indices (see ASTM card No. 9-432). By contrast, Fig. 6 curve (a) (no fluorine) shows only two peaks in the same 2Θ range; lines attributed to the Miller's indices [112] and [211] are not separated from each other. In Fig. 6 curve (b), possessing only a small fluorine concentration, the peak attributed to these two Miller indices is notably broadened. In all samples investigated, the lattice constants a_0 were higher, and the lattice constants c_0 lower than the values reported in ASTM card or observed at conventionally produced hydroxyapatite. Fig. (7) shows the lattice constant a_0 versus the fluorine content of the apatite. For hydroxyapatite without any fluorine doping, the lattice parameter a_0 is fairly different from that reported in the ASTM card. The higher the fluorine content, the smaller the lattice distortion and hence the deviation from the value listed in the ASTM card (see dashed line in Fig. (7)). Line-splitting was never observed, and also a detailed XRD line analysis gave no evidence for the occurrence of two separate hydroxyapatite and fluoroapatite phases.

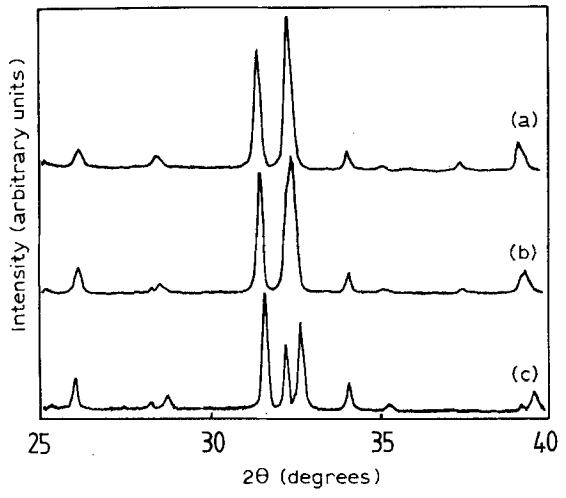

Figure 6 XRD patterns of calcined samples possessing different fluorine contents: (a) 0 wt %; (b) 0.1 wt %; (c) 0.6 wt % (calcination temperature 1100 °C, soak 5 h).

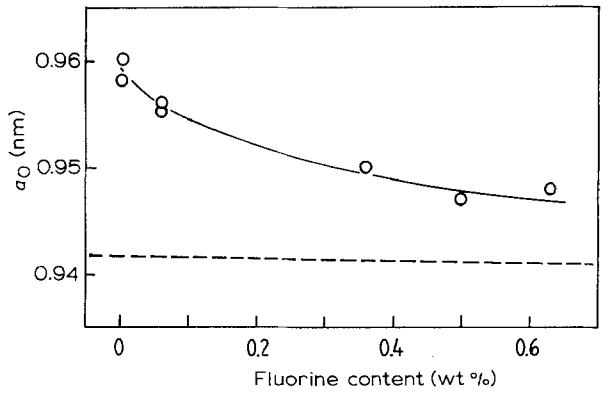

Figure 7 Lattice constant a_0 of hydroxyapatite/fluoroapatite solid solutions with different fluorine content (calcination temperature 1100 °C; soak 5 h).

4. Conclusions

In order to achieve the formation of hydroxyapatite/fluoroapatite solid solutions, a combination of two pyrolytic routes recently developed for the formation of hydroxyapatite and calciumfluoride was used. This led to the formation of apatites which, as far as can be detected from XRD, were not contaminated by additional phases, such as calcium fluoride or tricalcium phosphate. The fluorine content was about 50% of that calculated from the quantity of calcium trifluoroacetate added. The solid solutions formed, possessed slightly shifted XRD lines, the lattice distortion, however, decreases with increasing calcination temperature, soaking time and fluorine content.

References

1. J. F. OSBORN, "Implantatwerstoff Hydroxylapatit" (Quintessenz Verlag, Berlin, 1985).
2. K. DE GROOT, in "Ceramics in surgery", edited by P. Vincenzini, (Elsevier, Amsterdam, 1983) p. 79.
3. *Biomaterials* **1** (1980) 47.
4. F. C. M. DRIESSEN, Ber. Bunsenges. Phys. Chem. **82** (1978) 312.
5. T. KANAZAWA, T. UMEGAKI, K. YAMASHITA, H. MONMA and T. HIRAMATSU, *J. Mater. Sci.* **26** (1991) 417.
6. L. L. HENCH, *J. Amer. Ceram. Soc.* **74** (1991) 1487.
7. B. M. TRACY and R. H. DOREMUS, *J. Biomed. Mater. Res.* **18** (1984) 719.
8. G. L. DE LANGE and K. DONATH, *Biomaterials* **10** (1989) 121.
9. G. L. DE LANGE, C. DE PUTTER, K. DE GROOT and E. H. BURGER, *J. Dent. Res.* **68** (1989) 509.
10. R. S. ROTH and T. NEGAS, "Phase diagrams for ceramists" (American Ceramic Society, Westerville, OH, 1983) p. 213.
11. T. S. B. NARASARAJU, *Indian J. Chem.* **10** (1972) 308.
12. J. F. OSBORN and H. NEWESELY, *Biomaterials* **1** (1980) 108.
13. T. BRENDEL, A. ENGEL, and C. RÜSSEL, *J. Mater. Sci. Mater. Med.* **3** (1992) 175.
14. C. RÜSSEL, *J. Mater. Sci. Lett.* **11** (1992) 152.

Received 29 June and accepted 19 November 1992